Molecular Dynamics and ^{2}H-NMR Study of the Influence of an Amphiphilic Peptide on Membrane Order and Dynamics

Katarina Belohorcová, Jin Qian, and James H. Davis
Department of Physics, University of Guelph, Guelph, Ontario N1G 2W1, Canada

ABSTRACT A molecular dynamics simulation of a fully hydrated model membrane consisting of 12 molecules of 1,2-dimyristoyl-*sn*-glycero-3-phosphocholine, one amphiphilic peptide with the sequence acetyl-Lys-Lys-Gly-Leu$_{16}$-Lys-Lys-Ala-amide, and 593 water molecules was performed for 1.06 ns (Belohorcova, K., J. H. Davis, T. B. Woolf, and B. Roux. 1997. *Biophys. J.* 73:3039–3055). The analysis presented here is primarily focused on the phospholipid component and the results are compared with experimental ^{2}H-NMR studies of the lipid component of mixtures of the same peptide and lipid at a molar ratio of 1:32, and with earlier studies of closely related peptide/lipid mixtures. The phospholipid chain and headgroup isomer populations and isomerization rates compare favorably with previous simulations and experimental measurements. Of particular interest is the effect of the peptide on the phospholipid headgroup and hydrocarbon chain orientational order calculated from the simulation, which also agree well with experimental measurements performed on this and closely related systems. Comparison of the experimental results with the simulations not only shows that there is significant agreement between the two methods, but also provides new insight into the effect of the peptide on the lipid dynamics. In particular, these results confirm that a membrane spanning peptide has little effect on lipid chain order, and bilayer thickness if its hydrophobic length closely matches the lipid hydrocarbon thickness. In addition, we find that the peptide can have a strong ordering effect if it is longer than the lipid hydrophobic thickness.

INTRODUCTION

Molecular dynamics (MD) simulations and nuclear magnetic resonance (NMR) provide largely complementary views of membrane molecular structure, orientational order, and dynamics. Current simulations of model membrane systems cover motional time scales in the nanosecond range and can provide a precise, detailed description of fast phospholipid chain and headgroup isomerization and internal peptide backbone fluctuations and side-chain motions. Studies of lipid and peptide molecular diffusion are also becoming possible as longer simulation times are being run.

Nuclear magnetic resonance spectroscopy of solids, or of other ordered systems such as lipid bilayers, can give precise values for the residual motionally averaged orientation-dependent nuclear spin interactions through the measurement of nuclear electric quadrupolar splittings, the anisotropic part of the chemical shift, or inter-nuclear dipolar couplings (Davis and Auger, 1999). The NMR spectroscopic time scale (or averaging time) varies from a few microseconds to hundreds of milliseconds, depending on the values of the residual couplings observed. Even though the time scales of MD simulations and NMR spectroscopy are very different, they provide a consistent picture of these complex membrane molecular systems.

Molecular dynamics simulations have been widely used to study lipid bilayer systems (Tobias et al., 1997; Tieleman et al., 1997; Pastor et al., 1991) and there have been significant improvements in the system size and simulation length for such studies (Essman and Berkowitz, 1999; Pasenkiewicz-Gierula et al., 1999). A number of recent simulation studies of membranes have examined the interactions between peptides or proteins and lipids and water. Our recent paper on the same peptide/lipid/water system (Belohorcova et al., 1997) examined in detail the structure and dynamics of the peptide, while this article examines more closely the phospholipid component and compares the simulations with NMR studies of the same system and related synthetic peptide/lipid/water systems. Other MD studies on membranes have looked at a poly-alanine peptide/lipid mixture (Shen et al., 1997), gramicidin A/lipid mixtures (Woolf and Roux, 1994a, 1996; Chiu et al., 1991), the bacteriophage pf1 coat protein (Tobias et al., 1993; Roux and Woolf, 1996), alamethicin channels (Tieleman et al., 1999a, b), melittin (Berneche et al., 1998), porin (Tieleman and Berendsen, 1998), bacteriorhodopsin (Edholm et al., 1995), the transmembrane domain of Erb-B2 (Duneau et al., 1999), and other peptide/lipid mixtures (Kerr et al., 1994; Damodaran et al., 1995; Huang and Loew, 1995).

Lipid/water mixtures, lipid/peptide/water mixtures, and lipid/protein/water reconstituted systems have also been widely studied by NMR spectroscopy and relaxation methods, primarily using isotopically labeled peptides, proteins, or lipids in order to define precisely the sites being monitored (Davis and Auger, 1999; Cross, 1994; Davis, 1991). 1,2-dipalmitoyl-*sn*-glycero-3-phosphocholine (DPPC) and 1,2-myristoyl-*sn*-glycero-3-phosphocholine (DMPC) are by far the most widely studied phospholipids, and detailed descriptions of both hydrocarbon chain and headgroup structure, orientational order, and dynamics have been ob-

Received for publication 21 July 1999 and in final form 12 September 2000.

Address reprint requests to Dr. James Davis, Dept. of Physics, University of Guelph, Guelph, Ontario N1G 2W1, Canada. Tel.: 519-824-4120 ext. 2659; Fax: 519-836-9967; E-mail: jhd@physics.uoguelph.ca.

0006-3495/00/12/3201/16 $2.00

tained using NMR techniques (Davis, 1991; Seelig and Seelig, 1980). Gramicidin A is the most extensively studied model of an integral membrane protein and ion channel, and NMR studies have provided a detailed description of its structure and dynamics (Davis and Auger, 1999; Ketchem et al., 1996; North and Cross, 1995). The series of amphiphilic synthetic peptides with sequences $K_2G[L_N]K_2A$-amide (the peptides with N = 16, 20, and 24 are referred to as peptide-16, peptide-20, or peptide-24) was initially designed to provide a simple model of an integral membrane protein to investigate more quantitatively the interactions between membrane proteins and lipids (Davis et al., 1983). Extensive studies of its influence on lipid order, phase behavior and dynamics, and of its own structure and dynamics (Davis et al., 1983; Huschilt et al., 1985, 1989; Morrow et al., 1985; Pauls et al., 1985; Prosser et al., 1992) have been performed, and it was the subject of a recent MD study investigating its structural stability and dynamics within the same fully hydrated DMPC bilayer described in the present article (Belohorcova et al., 1997). The NMR results show that peptide-24 has a much stronger effect on DPPC chain order than peptide-16 does, but that peptide-16 does have a strong effect on DMPC chain order. The quantitative measurement of hydrocarbon chain order can be used to deduce the mean bilayer hydrophobic thickness (Schindler and Seelig, 1975; Douliez et al., 1995; Nagle, 1993). The hydrophobic core of peptide-24 is much longer than that of peptide-16, ~36 Å compared to 24 Å for peptide-16. The hydrophobic thickness of a pure DMPC bilayer 10°C above its phase transition temperature is reported to be ~25.4 Å (de Planque et al., 1998), which is close to the length of the hydrophobic core of peptide-16, but is much shorter than the length of the hydrophobic core of peptide-24. The core of peptide-16 is, however, a little longer than the 22.5 Å hydrophobic thickness of a pure DMPC bilayer (de Planque et al., 1998). Harroun et al. (1999a, b) argue that the gramicidin A dimer has a length of ~26 Å and that, at a lipid to peptide mole ratio of 10:1, it increases the DMPC bilayer thickness by ~1.5 Å. These results are in complete agreement with the effects reported here. There have been a number of other studies showing the importance of hydrophobic mismatch between peptide and lipid on membrane properties and function (Mouritsen and Bloom, 1984; Lewis and Engelman, 1983; Brown, 1994; Dumas et al., 2000; Morein et al., 2000).

In this article we complete the analysis of this acetyl-Lys_2-Gly-Leu_{16}-Lys_2-Ala-amide/DMPC/water system by carefully examining the phospholipid order and dynamics and comparing the simulation results with NMR spectroscopic measurements on pure lipid/water systems, and on synthetic peptide/lipid/water systems with compositions similar to those used in the simulation. The increases in lipid chain order observed by NMR are consistent with the simulation results. Comparison of peptide-16/DMPC mixtures with peptide-16/DPPC and peptide-24/DPPC mixtures reveals that peptide-16 has a much stronger effect on DMPC chain order than it has on DPPC order. Similarly, peptide-24 has a strong effect on DPPC chain order. We conclude that a trans-membrane peptide that is longer than the equilibrium lipid bilayer thickness induces significant ordering in the lipid chains to try to thicken the bilayer. The next section describes some of the details of the construction, equilibration, and simulation phases of the calculation and presents the experimental procedures used for the NMR studies. The Results and Discussion section describes and compares in detail the peptide backbone order and the phospholipid headgroup and hydrocarbon chain order and dynamics from the perspectives of the two techniques. The concluding section briefly discusses the questions which can soon be more fully addressed when simulations having both longer time scales and larger unit cells can be performed.

MATERIALS AND METHODS

Construction of the initial configuration for the simulation

The membrane model studied was composed of a synthetic peptide acetyl-Lys_2-Gly-Leu_{16}-Lys_2-Ala-amide, surrounded by 12 DMPC molecules (6 in each leaflet) and fully hydrated by 593 water molecules, corresponding to 51% water by weight, resulting in a total of 3613 atoms. The system construction, molecular dynamics simulation, and a subsequent analysis were performed by using the molecular mechanics software CHARMM (Brooks et al., 1983) and the all-atom force field PARAM 22 (Mackerell et al., 1992). The system construction approach described in detail by Woolf and Roux (1996) and by Roux and Woolf (1996) was used. This method significantly reduces the time needed for the equilibration step by assembling the system from its preequilibrated components. The detailed construction of the system was described elsewhere (Belohorcova et al., 1997; and Belohorcova and Davis, 1998).

Computational details

Both the equilibration and the simulation were performed in the NVE ensemble. Lengths of all the bonds containing hydrogens were constrained to a fixed value by the SHAKE algorithm (Ryckaert et al., 1977), therefore a relatively large integration step of 2 fs could be used. Nonbonded interactions were calculated using a group-based cutoff (Brooks et al., 1983) with a switching function and were updated every 5 time steps. The switching function was turned on at 10 Å and turned off at 12 Å; no nonbonded interactions were calculated beyond 13 Å. The dielectric constant was set to 1.0. Atom coordinates were saved every 50 fs throughout the trajectory production period.

Equilibration

The total length of the equilibration stage was 190 ps. For the first 50 ps the system was weakly coupled to a heat bath set at a temperature of 300 K with a friction coefficient of 3.0 ps^{-1} by using Langevin dynamics in order to speed up the approach to equilibrium. During this 50-ps period the positions of the peptide backbone and the C_2 atoms of the lipid glycerol were fixed. In the following 50 ps the temperature of the system was increased to 325 K in order to be well above the gel-to-liquid crystal transition temperature for DMPC, 24°C (Hinz and Sturtevant, 1972; Morrow and Davis, 1988). From this point on throughout the rest of the

equilibration the Verlet algorithm was used (Verlet, 1967). During this period the velocities were rescaled by a single factor when the temperature deviated by more than ±5 K from the equilibration temperature. The positional constraints on the selected atoms were also gradually removed. Then the system was equilibrated for another 90 ps, during which only the center of mass of the peptide was constrained by a cylindrical potential to the origin of the coordinate system coinciding with the center of the bilayer.

Simulation

The total length of the simulation stage itself was 1060 ps. Throughout the simulation the Verlet algorithm was used (Verlet, 1967). No coupling to a heat bath was imposed, as we wished to follow the unconstrained dynamics of the system without any complications that might arise due to this coupling (Leach, 1997; Rappaport, 1995; Feller et al., 1995). The only constraint maintained during the simulation was that the center of mass of the peptide was constrained by a cylindrical potential to the origin of the unit cell.

The evolutions of the total energy and of its individual contributions, the kinetic and the potential energies, were monitored throughout the equilibration and the simulation in order to determine whether the system had reached equilibrium. Because the simulation was performed in an NVE ensemble with no contact to a thermal bath, the total energy was expected to be constant. However, the energy was observed to increase slowly, in a stepwise fashion, with fairly long periods at a constant value with a total change over the length of the simulation of ~10% (Belohorcova et al., 1997). Both the kinetic and the potential energies contributed to the increase of the total energy. The most probable sources of this energy increase may be due to the finite time step of 2 fs, accumulation of numerical and round-off errors, or to the choice of an NVE rather than a constant pressure simulation system (see Pastor and Feller, 1996). The average temperature of the simulation was calculated to be 335.5 K with a root-mean-square (rms) deviation of 9.4 K.

Analysis

Radial distribution function

The radial distribution function gives the probability of finding an atom of type "i" around an atom of type "j" as a function of radial distance r_{ij}. It is the ratio of the local density $\rho_i(r_{ij})$ to the system density of the "i" atoms, ρ_i (Haile, 1992). The solvation of selected atoms by water is quantified in terms of this radial distribution function $g_{ij}(r_{ij})$

$$g_{ij}(r_{ij}) = \frac{\Delta N(r_{ij})}{\rho_i \Delta V(r_{ij})} \quad (1)$$

where

$$\Delta V(r_{ij}) = \frac{4\pi}{3}((r_{ij} + \Delta r_{ij})^3 - r_{ij}^3)$$

$\Delta N(r_{ij})$ is the number of waters i in a spherical shell of thickness Δr_{ij}, r_{ij} is the distance between the atom j and the spherical shell, and ρ_i is the bulk density of water molecules i.

NMR sample preparation and experiments

NMR experiments were performed on a home-built spectrometer in a magnetic field of 8.5 T, corresponding to a ^{2}H-NMR frequency of 55.26 MHz. The quadrupolar echo sequence (Davis et al., 1976) with CYCLOPS phase cycling (Hoult and Richards, 1975) were used for all deuterium spectra. The powder samples were prepared by mixing a total of ~50 mg of chain perdeuterated 1,2-dimyristoyl-*sn*-glycero-3-phosphocholine (DMPC-d_{54}) with H_2O at a 1:20 mole ratio, or peptide-16:DMPC-d_{54}:H_2O in a molar proportion of 1:32:640. For all the ^{2}H-NMR spectra the 90° pulse length used was 7.5 μs, with an echo delay of 35 μs and a recycle time of 0.25 s. For the powder samples 3600 scans were accumulated, while for the oriented peptide-16:DMPC-d_{54} sample 100,000 scans were acquired. Oriented samples were prepared as described by Prosser et al. (1994) by codissolving peptide and lipid in methanol, applying the solution to thin, pre-cut glass plates, drying, and they hydrating through a ^2H_2O saturated vapor phase. The plates were then redried using a vacuum and then rehydrated, again with ^2H_2O vapor, and incubated in this vapor phase at 50° for several days. It was found that carefully applying a drop of ^2H_2O to the top of each plate greatly accelerated the annealing process. The peptide/lipid plates become transparent when the mixture is well oriented. At this point the plates were carefully stacked within an 8-mm NMR sample tube. Excess sample mixture at the edges of the plates was carefully removed. The sample tube was mounted horizontally in the NMR probe with the normal to the plates oriented perpendicular to the applied magnetic field. The oriented sample peptide spectra were obtained using a long, soft inversion pulse centered at the water peak followed by a time delay allowing the water signal to recover to zero, at which time the quadrupolar echo sequence was applied.

RESULTS AND DISCUSSION

Density profile

The time-averaged density profile of the main components of the system projected along the bilayer normal, i.e., the z-distribution of the peptide, phosphorus, nitrogen, and glycerol of the lipid headgroups, lipid chains, and water, is shown in Fig. 1. It can be observed that the peptide spans a range extending from $\sim z = -22$ Å to $z = 20$ Å along the bilayer normal (the center of the bilayer is at $z = 0$ Å). The principal deviation from symmetry, aside from the orientation of the peptide electric dipole moment, is at the two ends of the peptide. At the N-terminus (located on the lower leaflet), the first three amino acid residues are Lys-Lys-Gly, and the two positively charged lysines extend into the water region in order to maximize the hydration of the side chains. At the C-terminus, however, the last three residues are Lys-Lys-Ala, and the lysines at this end, though more deeply buried within the bilayer, still tend to extend into the water region (Belohorcova et al., 1997). The z-coordinates of the phosphorus and the nitrogen in the lipid headgroups cover almost the same region in both leaflets, indicating that the PN vector is almost parallel to the bilayer surface. The distribution of the hydrocarbon chain density has a pronounced minimum in the center of the bilayer consistent with experimental measurements (Franks, 1976; Finean et al., 1978; Nelander and Blaurock, 1978; Wiener and White, 1992a; Nagle et al., 1996). At the lipid-water interface there is some overlap between hydrocarbon chain density and water density in the region of the lipid glycerol backbone.

In order to monitor permeation of water into the bilayer the z-coordinates of all the water oxygens in the system were calculated each 5 ps throughout the simulation. During the simulation no water molecules were able to diffuse

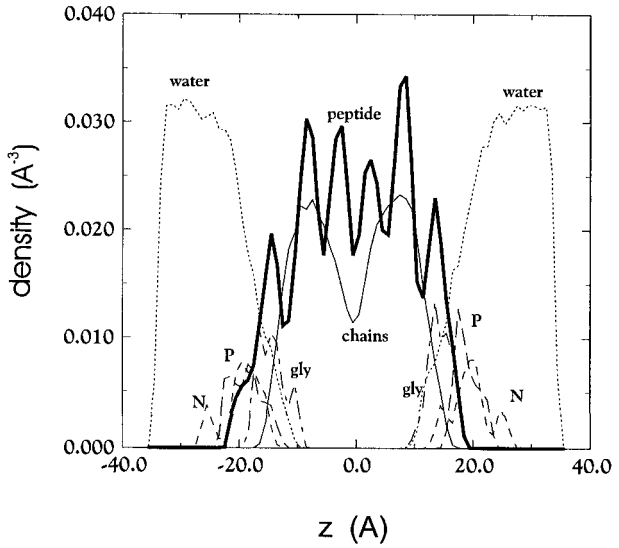

FIGURE 1 The MD simulation density profiles of water (*dotted line*), peptide (*thick solid line*), hydrocarbon chains (*thin solid line*), trimethylamine group (*dashed line*), phosphodiester group (*long dashed line*), and ester groups (*dotted-dashed line*) along the bilayer normal (the *z* axis). The center of the bilayer is at $z = 0$ Å. The density units are defined such that the graph for water gives the number of molecules per Å^3. Key features are the slight asymmetry in the peptide profile due to the different sequence at the two ends, and the overlap between the phosphodiester density and the trimethylamine group density near the lipid/water interface.

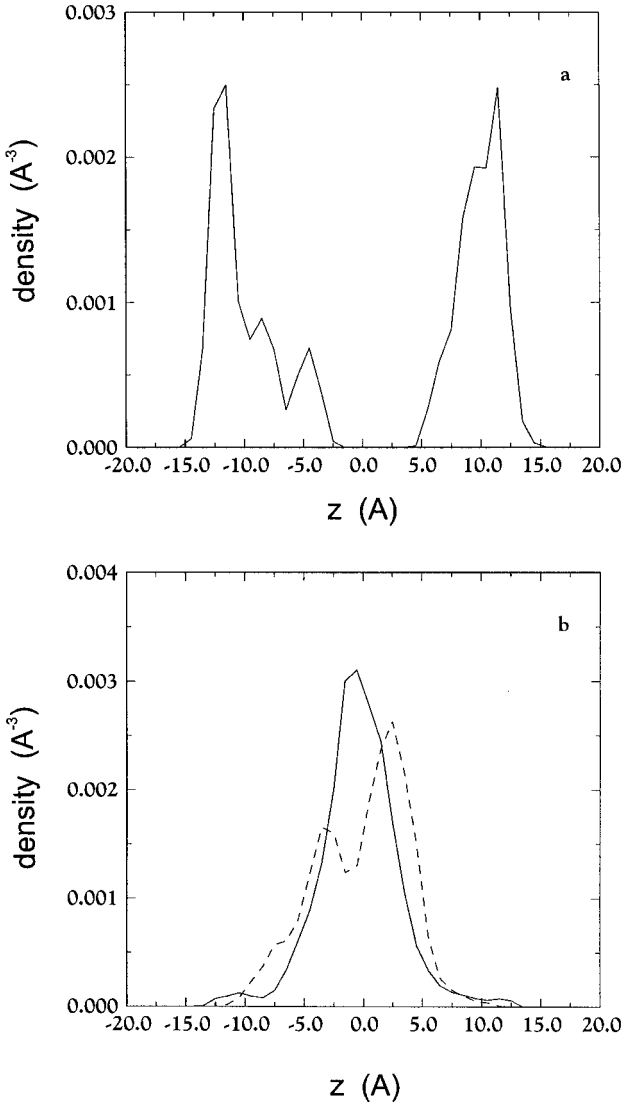

FIGURE 2 (*a*) The MD simulation density profile of carbon 6 of the *sn*-2 chain. (*b*) The density profiles of the carbon atoms of the methyl groups of both the *sn*-1 chain (*solid line*) and the *sn*-2 chain (*dashed line*). The center of the bilayer is at $z = 0$ Å and the density units are defined as for Fig. 1. Carbons near the lipid/water interface are relatively well localized, having narrow *z*-distributions compared to carbons near the terminal methyl group.

across the membrane, and the deepest penetration was to within 4 Å of the center of the bilayer (at $z = 0$ Å).

The *z*-distributions of all of the carbon atoms of both the *sn*-1 and the *sn*-2 chains were calculated in order to obtain detailed information on the average order within the hydrocarbon region of the lipid bilayer. Comparison of the carbon *z*-distributions of the *sn*-1 and *sn*-2 chains shows that the corresponding carbon atoms in the respective chains do not occupy the same *z*-region due to the bend of the *sn*-2 chain, which occurs near the first CH_2 segment of the hydrocarbon chain with the result that this chain does not penetrate as deeply into the bilayer as the *sn*-1 chain which runs, on average, roughly parallel to the bilayer normal (Seelig and Seelig, 1980). The *z*-distributions of the individual carbon atoms are spread over a range of at least 10 Å due to the high degree of chain flexibility or disorder. As expected, carbon atoms closer to the headgroups had narrower *z*-distributions compared to those near the terminal methyl groups, which had the widest *z*-distribution observed for any chain position. The distribution for the methyl group of the *sn*-1 chain covers the *z*-region from ~ -12 to ~ 12 Å, with its maximum centered at 0 Å, the center of the lipid bilayer (see Fig. 2 *b*). This indicates some degree of interpenetration of the tails into the opposing leaflets. Two small maxima can be observed at $\sim \pm 10$ Å, probably indicating the limit for methyl group excursions toward the lipid-water interface. The *z*-distribution of the methyl group of the *sn*-2 chains has two maxima, centered at ± 3 Å, because the *sn*-2 chain penetrates less deeply into the bilayer compared to the *sn*-1 chain.

^{2}H-NMR spectrum of the peptide

The angles between individual N–H bonds and the peptide helix axis can be calculated as a function of time, and the average value $\langle (3\cos^2\theta_{NH} - 1)/2 \rangle$ for each bond can be determined (the angle brackets indicate the time average over the simulation). From these time averages a ^{2}H-NMR spectrum of the peptide can be simulated and compared to

the experimental spectrum. It should be emphasized that the time scales of the MD method and of the ^{2}H-NMR experiment differ by several orders of magnitude, and thus care must be taken when comparing simulated and experimental spectra.

Assuming fast, axially symmetric motion about the helix axis, with the helix axis aligned parallel to the bilayer normal, the ^{2}H-NMR spectrum in this case can be simulated using only the deuterium quadrupolar splitting $\Delta\nu_Q$ which, in the presence of axially symmetric motion, can be expressed as (Prosser et al., 1994)

$$\Delta\nu_Q = \tfrac{3}{4}\frac{e^2qQ}{h}(3\cos^2\theta - 1)$$
$$\tfrac{1}{2}\langle(3\cos^2\theta_D - 1) + \eta\cos 2\phi_D \sin^2\theta_D\rangle \quad (2)$$

where e is the electronic charge, Q is the nuclear quadrupolar moment, eq is the principal value of the electric field gradient (EFG) tensor, h is Planck's constant, and η is the electric field gradient asymmetry parameter. The Euler angles ϕ_D, θ_D, ψ_D define the transformation of the EFG tensor from its principal axis system to the diffusion tensor system, where the z'-axis is aligned along the helix axis (assumed to be parallel to the bilayer normal). The Euler angle θ defines the transformation from the diffusion tensor system to the laboratory frame having its z axis along the static magnetic field. The angle brackets represent a time average over motions that are fast compared to the quadrupolar splitting.

The principal axis of the electric field gradient tensor is aligned nearly along the N-^{2}H bond (Prosser et al., 1994) and the asymmetry parameter η, though appreciable for N-^{2}H bonds, has a relatively small effect on the measured splittings. When θ_D, the angle between an N–H bond and the helix axis is small, the effect of η is also quite small because of the $\sin^2\theta_D$ term in Eq. 2. For amino acids near the center of the helix $\sin^2\theta_D \sim 0.15$, while for those near the ends of the helix this factor can be considerably larger (e.g., $\sin^2\theta_D \sim 0.6$ at the N-terminus and $\sin^2\theta_D \sim 0.3$ at the C-terminus). Thus the effect of η will be small for those positions with large splittings, but may be important for those positions with small splittings. In order to include the effect of η, it would be necessary to know the principal values and the orientation of the EFG tensor within the peptide for each N-^{2}H bond. For simplicity, the asymmetry parameter η (which experimentally has a value between 0.1 and 0.2 for amides) was set to zero in the spectrum simulations performed here. If it is further assumed that the helix axis is parallel to the bilayer normal and that the bilayer normal is oriented along the magnetic field, i.e., in the z-direction in the laboratory frame, then the expression for the quadrupolar splitting is simplified to the following form:

$$\Delta\nu_Q = \nu_Q\langle(3\cos^2\theta_{NH}(t) - 1)\rangle \quad (3)$$

where

$$\nu_Q = \frac{3}{4}\frac{e^2qQ}{h} \quad (4)$$

is the static quadrupole coupling constant. A value of 150 kHz was used for ν_Q, which is typical for rigid amide deuterons that are hydrogen-bonded to oxygen atoms in crystalline solids (Pauls et al., 1985). Table 1 shows the deuterium quadrupolar splittings of individual N–^{2}H bonds calculated from the simulation.

Using these values and Eq. 3 to calculate the corresponding quadrupolar splittings, the ^{2}H-NMR spectrum of the peptide amides was calculated by superposing contributions from each of the amide positions. The peaks with large quadrupolar splittings in the simulated spectrum, Fig. 3 *b*, and in the experimental spectrum, Fig. 3 *a*, match quite well, while the peaks with small splittings in the simulated spectrum are shifted with respect to the peak positions in the experimental spectrum. This could be partly due to the neglect of the EFG asymmetry parameter or to neglect of longer time scale motions (beyond 1 ns). Finally, the water suppression used in obtaining the experimental spectrum also would eliminate any peptide peaks having quadrupolar splittings of ~5 kHz or smaller.

Presumably, the most important difference between the simulated and experimental spectra arises from the difference of the time scales. The experimental time scale of ^{2}H-NMR spectroscopy is on the order of microseconds or

TABLE 1 Angle between the NH bond and the helix axis for all amino acid residues in the peptide and the calculated deuterium quadrupolar splittings, averaged over the simulation trajectory

Peptide Residue	$\langle\theta_{NH}\rangle$ (deg)	RMS Fluct. of $\langle\theta_{NH}\rangle$ (deg)	$\Delta\nu_Q$ (kHz)
Lys	128.93	16.14	34.14
Lys	123.16	16.30	1.78
Gly	116.51	14.13	−42.13
Leu	140.13	14.65	111.66
Leu	150.14	12.15	178.77
Leu	161.97	9.92	247.17
Leu	148.80	12.68	169.95
Leu	150.01	11.14	178.52
Leu	158.13	8.06	231.43
Leu	161.84	9.43	247.10
Leu	155.25	11.35	210.37
Leu	152.67	8.59	199.15
Leu	161.94	9.96	246.75
Leu	163.57	8.67	255.79
Leu	155.32	11.16	210.90
Leu	152.69	7.49	200.85
Leu	160.13	11.49	235.69
Leu	161.19	10.03	243.55
Leu	156.45	10.35	218.89
Lys	139.48	10.69	107.85
Lys	142.98	11.40	132.78
Ala	150.77	10.44	185.64

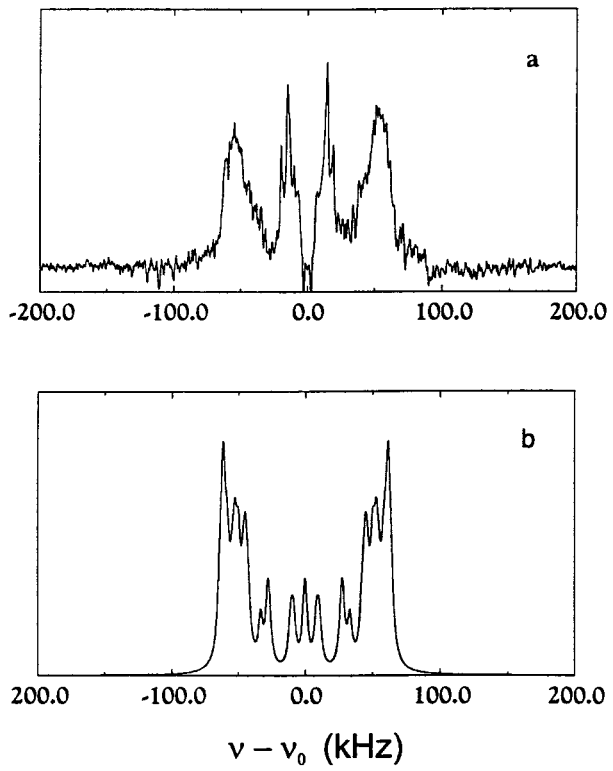

FIGURE 3 (*a*) The experimental ^{2}H-NMR spectrum of an exchange-labeled peptide-16/DMPC/^2H_2O sample oriented with the bilayer normal at 90° relative to the magnetic field. The spectrum was taken using the quadrupolar echo sequence using 7.5-μs pulses and a 35-μs echo delay, with water suppression, at a deuterium Larmor frequency of 55.26 MHz. (*b*) A simulated ^{2}H-NMR spectrum of the peptide. The Lorentzian line broadening used in the simulation corresponds to a value of $T_2 = 0.5$ ms. The loss of intensity due to evolution during the 90° pulses was not included in the simulation.

longer and the experimental spectrum reflects the time-averaged motion of the NH bonds over that time scale. The much shorter time scale of the simulation (1 ns) can only incompletely sample most of the peptide motions, and therefore cannot reflect the motional averaging occurring on longer time scales. Other important motions, such as axial diffusion about the peptide's long axis and the slow reorientation of the helix axis relative to the bilayer normal (Prosser and Davis, 1994), have not been explicitly included in the simulation (the axial diffusion was assumed, however, in order to allow us to compare with a sample oriented at 90° relative to the bilayer normal). Such whole molecule reorientations could be included empirically by scaling all of the simulated quadrupolar splittings by a single constant factor. In addition, motions whose time scales are of the order of the inverse of the quadrupolar splittings can result in strong broadening of the resonances, and this effect cannot be easily taken into account without more detailed knowledge of the nature of these slow motions.

Lipid chains

Structure and dynamics of lipid chains

A dihedral angle ϕ_i was defined by four consecutive carbon atoms ($C^iC^{i+1}C^{i+2}C^{i+3}$) in the lipid chain and describes the rotation about the $C_{i+1}C_{i+2}$ bond (for the carbon atom and dihedral angle notation see Sundaralingam, 1972). Fluidity of a biological membrane is a direct consequence of the flexibility of lipid chains caused by frequent transitions of lipid chain dihedral angles among one of the three stable states, the *trans* state (corresponding to the potential minimum at 180°), the *gauche*$^+$ state (corresponding to the potential minimum at +60°), and the *gauche*$^-$ state (corresponding to the potential minimum at −60°) (Cevc and Marsh, 1987). Even though the present simulation was very short compared to the time scale of many of the lipid motions, isomerizations of dihedral angles occur on the order of tens to hundreds of picoseconds (Cevc and Marsh, 1987), a time scale adequately covered by the simulation. The dynamics of a hydrocarbon chain can be characterized, to some extent, in terms of dihedral angle transitions between individual states corresponding to potential energy minima. In order to avoid counting a large fluctuation as a true transition, a transition was counted only when the dihedral angle crossed the energy barrier and reached the bottom of the potential well (±5°) of the new configuration (Helfand, 1978). This method can, however, overcount isomerizations if one counts recoils and overshoots as a transition. Therefore, a successful transition of a dihedral angle to a new state was assumed to occur only when its residence time in the new state was at least 2 ps (Zhang and Pastor, 1994). The same criterion was used to identify the state in which any given dihedral angle resides.

In the gel phase, the lipid hydrocarbon chains are essentially in an all-*trans* fully extended conformation. In the liquid-crystalline phase the lipid bilayer is disordered due to the increased content of *gauche* conformations in lipid chains. The fraction of *gauche* states fluctuates about an average value of 0.22 for the *sn*-1 chain and a value of ~0.23 for the *sn*-2 chain. This translates into an average of ~2.4 *gauche* states per *sn*-1 chain and ~2.6 *gauche* states per *sn*-2 chain. The difference is primarily due to the more or less permanent bend of the *sn*-2 chain at the first methylene group. The results compare well with the results of Robinson et al. (1994) who estimated the average number of *gauche* states in the *sn*-1 chain of DMPC at 323 K to be 2.6 and in the *sn*-2 chain to be 2.5. Chiu et al. (1995) who performed simulations on DMPC/water with non-zero surface tension (56 dynes/cm for the bilayer) also obtained ~25% *gauche* and 75% *trans* conformers. Simulations of DPPC water mixtures (Egberts et al., 1994) at 335 K and of a single molecule of DPPC with stochastic boundary conditions in an orienting potential at 324 K (De Loof et al., 1991) and in monolayers (Ahlstrom and Berendsen, 1993) obtained similar *gauche*/*trans* fractions. Experimental mea-

TABLE 2 Fraction of *gauche* states per individual dihedral angle

Dihedral Angle	*sn*-1 Chain	*sn*-2 Chain
ϕ_1	0.23	0.77
ϕ_2	0.30	0.16
ϕ_3	0.17	0.15
ϕ_4	0.26	0.19
ϕ_5	0.13	0.18
ϕ_6	0.23	0.12
ϕ_7	0.21	0.19
ϕ_8	0.21	0.17
ϕ_9	0.22	0.19
ϕ_{10}	0.21	0.19
ϕ_{11}	0.24	0.26

A short-hand notation for the dihedral angles is used where only the first of the four consecutive carbon atoms defining a dihedral angle is given (the numbering of carbon atoms follows the notation of Sundaralingam, 1972).

surements of *gauche* populations for DPPC are in good agreement, with between 3.6 and 4.2 *gauche* states per lipid (both chains) reported from infrared spectroscopy measurements (Mendelsohn et al., 1989; Mendelsohn and Snyder, 1996), ~4.3 per lipid deduced from deuterium NMR measurements (Seelig and Seelig, 1974, 1980), and 5.2 per lipid from Raman spectroscopy (Pink et al., 1980).

The fraction of *gauche* states for each of the individual dihedral angles was calculated for both chains, and the data are summarized in Table 2. Because the *sn*-2 chain is bent near the first methylene group, it is not surprising that the ϕ_1 dihedral angle of the *sn*-2 chain occupied the *gauche* state for 77% of the simulation. By comparison, the ϕ_1 dihedral angle of the *sn*-1 chain spent the major part (77%) of the simulation in the *trans* state. Contrary to expectations, for the *sn*-1 chain the highest fraction of *gauche* states occurs for ϕ_2 while the methyl end groups of both chains also exhibit high fractions of *gauche* states.

The average lifetimes of the *trans* (τ_t) and *gauche* (τ_g) states were calculated for individual dihedral angles for both chains using the expression (van der Ploeg and Berendsen, 1983)

$$\tau_t = 2f/n$$

$$\tau_g = 2(1 - f)/n$$

where f is the fraction of the *trans* states and n is the average number of transitions per picosecond. The mean lifetimes as a function of chain position are summarized in Table 3. Moving down the chain toward the terminal methyl, both the lifetimes τ_t and τ_g decrease, as expected, with τ_t always being longer than τ_g. The isomerization rates, κ, were calculated by counting the total number of isomerizations occurring at a given position and dividing by the total simulation time (Venable et al., 1993). The individual values are also summarized in Table 3. The isomerization rates are the largest for ϕ_{10} and for ϕ_{11}, reflecting the increased mobility at the lipid tail ends. Fig. 4 illustrates the difference in the transition rates of the dihedral angle ϕ_1 and of the dihedral angle ϕ_{11} for the *sn*-2 chain of one of the lipid molecules (DMPC 9). The ϕ_1 angle spends most of the simulation time in the *gauche*$^-$ state, consistent with the bend at this position, with two short-lived transitions to the *trans* state. However, the dihedral angle ϕ_{11} exhibits many transitions between the *trans* and the *gauche*$^+$ and *gauche*$^-$ states.

The isomerization rates for this DMPC/peptide mixture are slightly higher than the isomerization rates of DPPC at 50°C reported by Venable et al. (1993). This may be due to the larger value of $T - T_m$, the difference between the simulation temperature and the chain melting transition temperature. For this simulation $T - T_m \approx 40$°C, while for Venable et al. (1993) it was ~9°C. Similar results were reported by De Loof et al. (1991) for a single DPPC molecule with stochastic boundary conditions. Analysis of ^{1}H- and ^{2}H-NMR relaxation data of peptide-16/DPPC mixtures found an effective *gauche*/*trans* transition rate of $\sim 4 \times 10^{10}$ s^{-1}, which is still in good agreement considering that the relaxation data are not very sensitive to this motion due to

TABLE 3 Average lifetimes τ_t and τ_g and the isomerization rates κ (see the text for the definition) of individual carbon atoms in the *sn*-1 and the *sn*-2 lipid chains

	sn-1 chain			*sn*-2 chain		
Dihedral Angle	τ_t (ps)	τ_g (ps)	κ (ns^{-1})	τ_t (ps)	τ_g (ps)	κ (ns^{-1})
ϕ_1	487.8	152.1	6.7	193.3	852.1	4.6
ϕ_2	92.5	42.7	31.3	204.8	40.2	16.4
ϕ_3	222.7	42.9	15.4	164.5	29.0	21.0
ϕ_4	110.5	38.2	27.2	170.5	38.9	19.2
ϕ_5	162.9	27.5	21.7	141.0	28.5	24.4
ϕ_6	114.1	35.7	17.2	190.8	25.6	18.9
ϕ_7	128.5	34.8	24.5	139.4	31.3	23.8
ϕ_8	114.1	31.1	27.8	118.2	23.6	28.3
ϕ_9	115.0	31.8	27.7	125.2	28.3	26.7
ϕ_{10}	80.4	20.5	40.3	87.7	21.4	36.5
ϕ_{11}	72.46	22.3	42.9	65.9	24.1	44.8

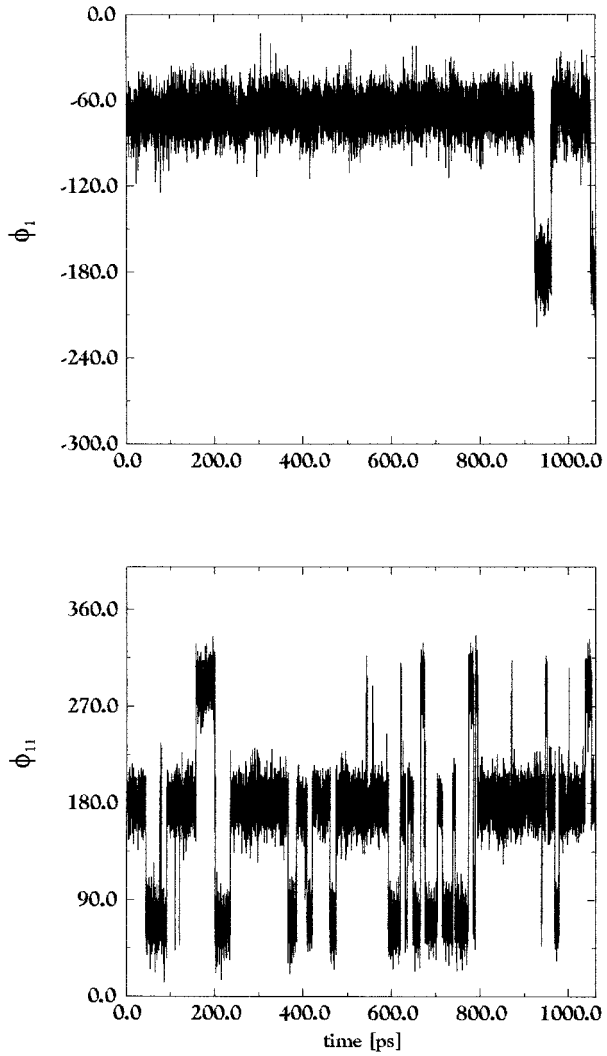

FIGURE 4 Comparison of the evolution of the ϕ_1 and ϕ_{11} dihedral angles for the *sn*-2 chain of DMPC 9. ϕ_1 is the dihedral angle for rotation about the C_2-C_3 bond, while ϕ_{11} is the rotation about the C_{12}-C_{13} bond. A value of $\pm 60°$ is indicative of a *gauche* conformer, while a value of $\pm$ 180° indicates a *trans* conformer.

competition with other important relaxation mechanisms (such as long axis diffusion) (Kimmich et al., 1983; Meier et al., 1986; Prosser et al., 1992).

The sequence of conformers $g^{\pm}g^{\mp}$, generally referred to as a *kink*, keeps the chain perpendicular to the bilayer surface because two *gauche* bonds of opposite sign separated by one *trans* bond displace the rest of the chain only by one bond that runs parallel to the bilayer surface. The average number of kinks was calculated to be 0.24 for the *sn*-1 chain and 0.22 for the *sn*-2 chain. This is lower than the number obtained by Stouch (1993), who calculated that there are from 0.5 to 1 kinks per DMPC chain at 320 K, and that of Robinson et al. (1994), who evaluated the mean number of kinks per dimyristoyl chain at 323 K to be 0.5. This may be an effect of the influence of the peptide on the lipid hydrocarbon chain mobility.

Order of the hydrocarbon region

The deuterium NMR quadrupolar splitting is proportional to the C-^{2}H bond order parameter S_{CD}, which is used to characterize the order of lipid hydrocarbon chains (Seelig and Seelig, 1980). It can be calculated from simulation trajectory files using the equation $S_{CD} = \frac{1}{2}\langle 3\cos^2\theta(t) - 1\rangle$, where $\theta(t)$ is the instantaneous angle between the direction of the C-^{2}H bond and the bilayer normal, at time t, and the angle brackets represent an average over the length of the simulation. Fig. 5 compares the simulated order parameters, averaged over all lipids, as a function of position on the chain, with the experimental order parameter profile obtained from ^{2}H-NMR quadrupolar echo experiments of a powder sample composed of a mixture of the peptide-16

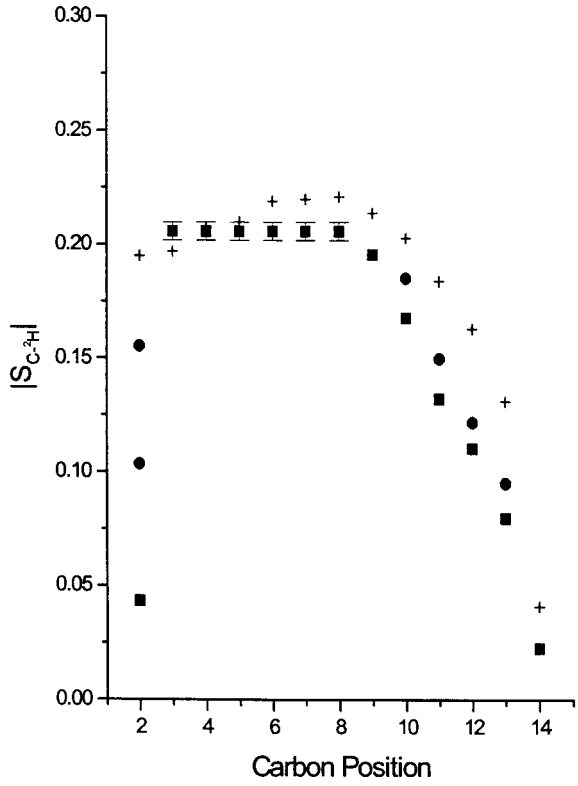

FIGURE 5 The order parameter profile of the hydrocarbon chains calculated from the simulation trajectory is shown by the "+" symbols. The peptide to lipid molar ratio for the simulation is 1:12. The filled circle and square symbols are the order parameters determined from the dePaked experimental ^{2}H-NMR spectrum obtained from a powder sample of peptide-16/DMPC-d_{54} at a peptide to lipid molar ratio of 1:32 at a temperature of 60°C. The use of two symbols for a given carbon position indicates that the two chains have inequivalent splittings at those positions. In such cases, the spectra do not permit the identification of which chain corresponds to which splitting, although generally the larger splitting is associated with the *sn*-2 chain.

chain perdeuterated DMPC (at a molar ratio of 1:32) and water at 60°C. The concentration of the peptide in the simulation was higher, corresponding to a peptide/lipid molar ratio of 1:12, which may explain the slightly larger order parameters obtained from the simulation for positions 6 to 14 (see Fig. 8 below).

The experimental order parameter profiles were obtained directly from the "dePaked" powder spectra (Bloom et al., 1981), such as those shown in Figs. 6 and 7, by measuring the quadrupolar splittings of all of the identifiable peaks in the spectra and assigning them by assuming that chain order increases monotonically from its minimum value at the terminal methyl group (center of the bilayer). These spectra demonstrate the sensitivity of the chain order parameters to temperature and peptide concentration. The experimental order parameter profiles determined by this method are in good agreement with those obtained by specific ^{2}H labeling of a pure DMPC/water mixture (Oldfield et al., 1978). The influence of peptide-16 on chain order is shown more quantitatively in Fig. 8, where the first moment of the ^{2}H-NMR spectrum (Davis, 1979, 1983) is plotted as a function of temperature for a pure DMPC/water dispersion (*filled squares*) and for the peptide-16/DMPC/water dispersion (*filled circles*). The first moment is proportional to the average value of S_C-^{2}H, so we can also compare these experimental values to the average order parameter calculated from the simulation (at a peptide to lipid ratio of 1:12 and at a temperature of 335 K), which is shown as the solid triangular point on the graph. The addition of ~3 mol % peptide-16 results in an increase in the average chain order parameter by ~6%. The value from the simulation at a peptide concentration of ~7 mol % is ~14% higher than that of the pure lipid at 60°C and ~7% higher than the 3 mol % sample. The roughly linear increase in lipid chain order with increasing peptide concentration for the DMPC/peptide-16 system is similar to that seen in mixtures of DPPC/peptide-24 (Huschilt et al., 1985), shown as filled squares in Fig. 9. Mixtures of peptide-16 in DPPC show quite different behavior, however, having a much weaker dependence on peptide concentration, as shown by the filled circles in the figure. This behavior suggests that the peptide has little effect on lipid chain order and bilayer thickness if its hydrophobic length is well matched to the equilibrium thickness of the lipid hydrocarbon region, but that the peptide has a strong ordering effect if it is longer than the equilibrium thickness of the lipid.

It is also possible that some of the difference between the experimental values of M_1 and the value calculated from the simulation results is due to the different time scales of ^{2}H-NMR and our simulation. ^{2}H-NMR gives M_1 values averaged over motions that are fast compared to 10^{-6} to 10^{-3} s^{-1}, while the simulation covers an interval of only 1 ns.

The order parameter profiles for the two bilayer leaflets were calculated separately to determine whether the difference in the amino acid sequence at the peptide termini affects the order parameters of the carbon atoms close to the lipid headgroups. Indeed, a difference was seen along the whole length of the chains, the order parameters being systematically lower in the lower leaflet where the N-terminus of the peptide is anchored, with the most pronounced effect near the lipid/water interface. The order

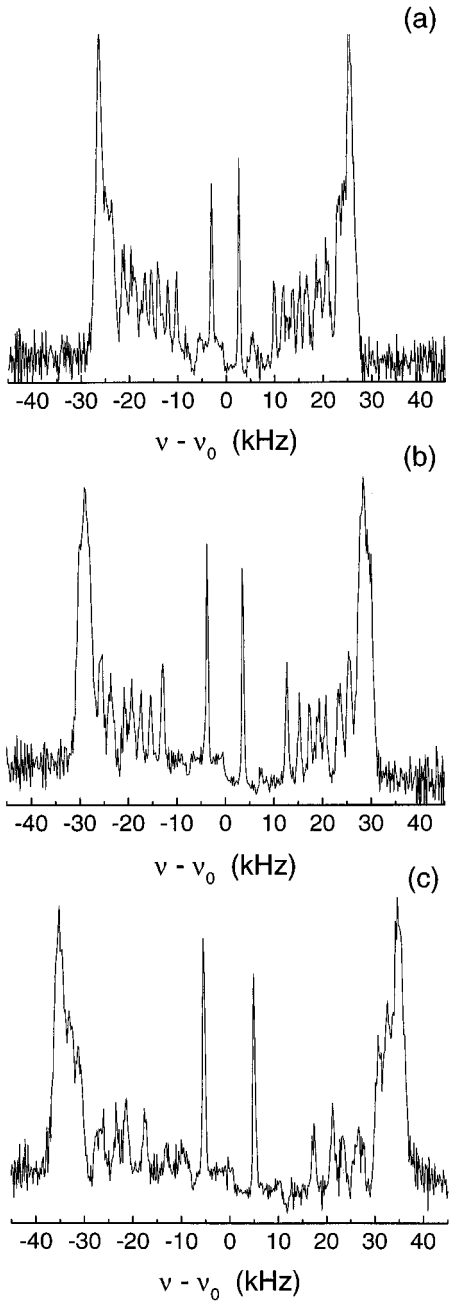

FIGURE 6 dePaked ^{2}H-NMR spectra of mixtures of peptide-16/DMPC-d_{54} at a peptide to lipid molar ratio of 1:32 at (*a*) 60°C, (*b*) 40°C, and (*c*) 25°C. The frequency scale gives the quadrupolar splittings corresponding to the 0° orientation of the bilayer normal relative to the static laboratory magnetic field.

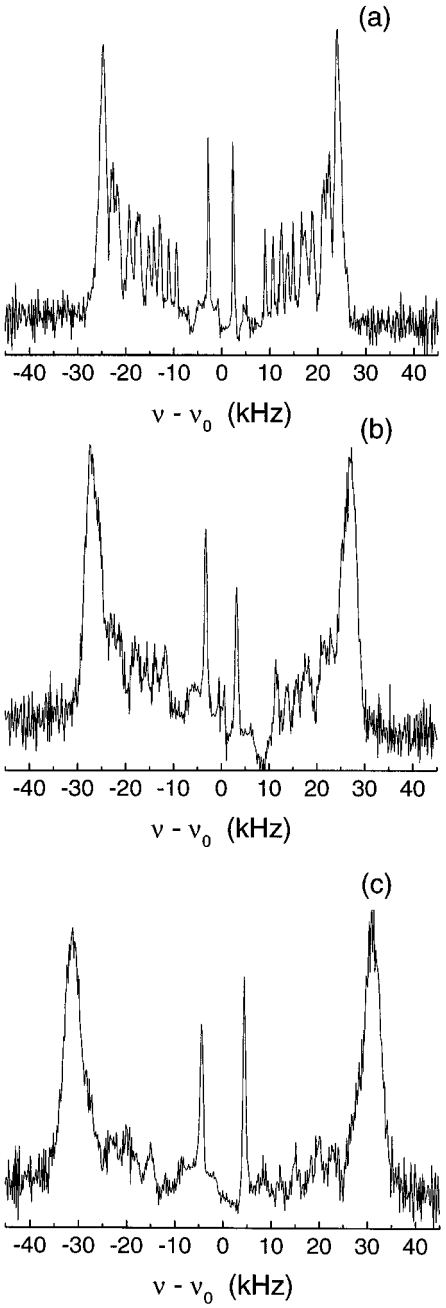

FIGURE 7 dePaked ^{2}H-NMR spectra of DMPC-d_{54} at (*a*) 60°C, (*b*) 40°C, and (*c*) 25°C. The frequency scale gives the quadrupolar splittings corresponding to the 0° orientation of the bilayer normal relative to the static laboratory magnetic field.

parameter profiles were also separately evaluated for both the *sn*-1 and the *sn*-2 chains. The *sn*-2 chain order parameter profile exhibited higher values compared to corresponding positions of the *sn*-1 chain, as expected from the bend of the *sn*-2 chain near its first methylene group. However, because of the small size of the simulation unit cell, it is possible that these differences are due to inadequate statistics.

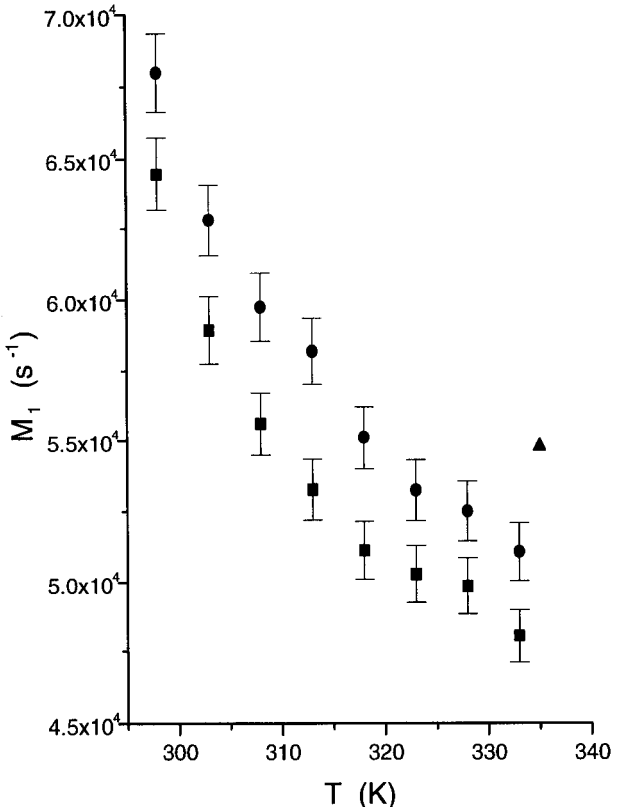

FIGURE 8 The temperature dependence of the first moment, M_1, of the ^{2}H-NMR powder pattern spectra of a mixture of peptide-16/DMPC-d_{54} at a peptide to lipid molar ratio of 1:33 (*filled circles*) and of DMPC-d_{54} (*filled squares*). The error bars show the estimated 1% random error in the values for M_1. The solid triangle symbol is the value of the first moment calculated from the average hydrocarbon chain quadrupolar splittings from the molecular dynamics simulation (corresponding to a peptide to lipid molar ratio of 1:12).

Lipid headgroups

The headgroup structure and mobility were investigated in terms of the states of the dihedral angles and the transitions between these states. Inasmuch as the synthetic peptide has a different amino acid sequence at its two termini, the analysis was performed separately for the upper and for the lower leaflets of the bilayer in order to see if this asymmetry has any effect on the headgroup structure or mobility. The dihedral angle definitions used are those of Sundaralingam (1972) and are shown in Fig. 10.

Orientation of PN dipoles in the lipid bilayer

The choline headgroup of a DMPC molecule possesses a large dipole moment that strongly interacts with water and other lipid molecules. The phosphorus to nitrogen (PN) vector defines the direction of the headgroup electric dipole moment. In the upper leaflet the average angle between the PN vector and the outward point bilayer normal was 84° ±

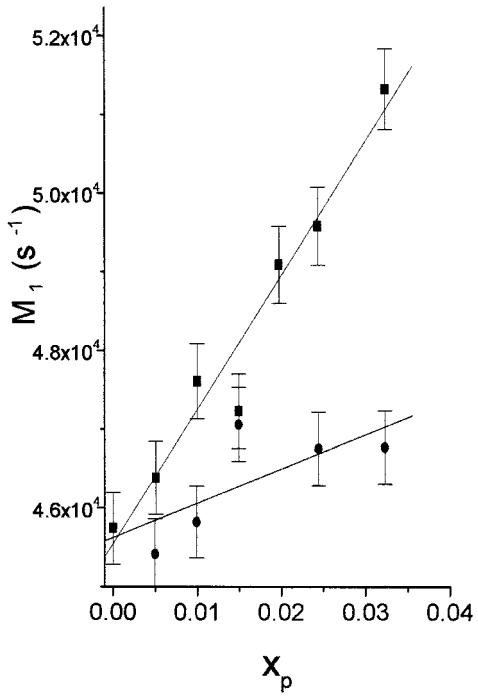

FIGURE 9 Comparison of the peptide concentration dependence of the first moment, M_1, of the ^{2}H-NMR powder pattern spectra of mixtures of peptide-16/DPPC-d_{54} (*filled circles*) and of peptide-24/DPPC-d_{62} (*filled squares*) at a temperature of 50°C. The solid lines are least squares fits to the data. Error bars show the estimated 1% random error in the values of M_1.

1.4°, and in the lower leaflet it was 80° ± 3.0° (the uncertainties give the rms deviations averaged over the full trajectory). The average angles for individual lipids in both leaflets ranged from 54° to 126°. The mean value for each of the leaflets is less than 90° so that, on average, the dipoles are pointing into the water and away from the lipid plane. The results are in good agreement with those of Marrink et al. (1993) who calculated the average orientation of the dipole vector in pure DPPC at 350K to be 20° with respect to the bilayer plane (i.e., 70° with respect to the bilayer normal). Experimental results also indicate that the average orientation of this vector is roughly within the bilayer plane (Seelig et al., 1977; Wiener and White, 1992b). The distribution of the PN angles measured with respect to the bilayer normal, and averaged over the length of the simulation and over the molecules in each of the two leaflets, are shown in Fig. 11.

The distributions in opposing leaflets differ, with the distribution of the lower leaflet being much broader compared with that of the upper leaflet. Although it is not possible to be certain, due to the small size of the system studied, this difference may be due to the differences in the amino acid sequence at the peptide termini. In particular, it may be a result of the different level of penetration of the peptide lysine side chains into the lipid region.

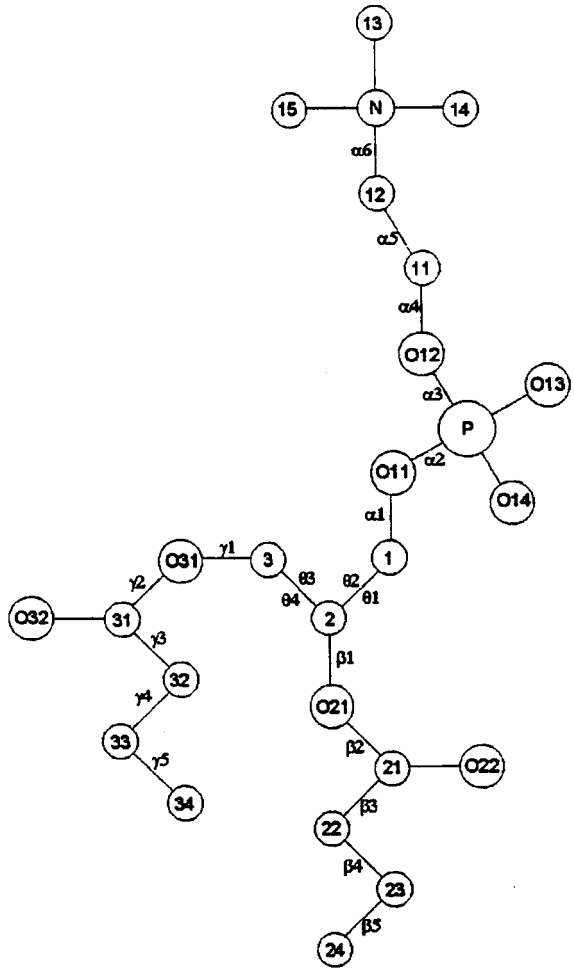

FIGURE 10 The DMPC glycerol backbone and headgroup structure showing the definitions of the dihedral angles and the atom numbering scheme used in the text, according to Sundaralingam (1972).

Structure and flexibility of lipid headgroups

The glycerol backbone is thought to be the most rigid part of the lipid headgroup (Hitchcock et al., 1975; Büldt and Wohlgemuth, 1981; Wiener and White, 1992b). Its motion was investigated in terms of four dihedral angles: θ_1 and θ_2, which define the rotation about the glycerol C_1C_2 bond, and θ_3 and θ_4, which define the rotation about the C_2C_3 bond (for the dihedral angle notation see Sundaralingam, 1972), as shown in Fig. 10. The isomerization rates of both the θ_1 and θ_2 dihedral angles (averaged over the whole simulation and over all lipids in an individual leaflet) were 1.3 ns^{-1} in the upper leaflet and 1.6 ns^{-1} in the lower leaflet. The isomerization rates of the θ_3 and θ_4 angles were 0.3 ns^{-1} in the upper leaflet, but no transitions were observed at all in the lower leaflet. The low isomerization rates of dihedral angles θ_1–θ_4 reflect the reduced mobility of the glycerol backbone relative to the rest of the molecule. The average occupancies of the glycerol backbone dihedral angles are

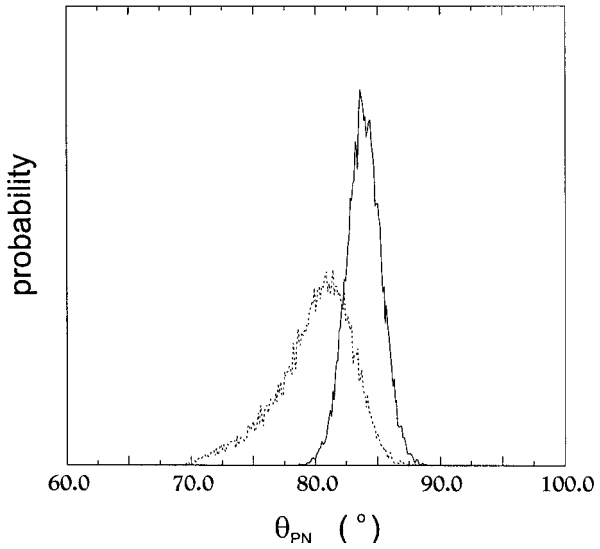

FIGURE 11 The distribution of the orientation of the PN electric dipole moment with respect to the bilayer normal in the upper leaflet (*solid line*) and in the lower leaflet (*dotted line*). These were calculated from the molecular dynamics simulation, averaging over all lipids in each leaflet.

summarized in Table 4. The most frequently occupied state of θ_1 appears to be the g^+ state in the upper leaflet and the *trans* state in the lower leaflet, although the g^+ and the *trans* states are almost equally populated in the lower leaflet. The angle θ_2 was in the *trans* state in the upper leaflet for most of the simulation, while in the lower leaflet it was in the g^- state. The angle θ_3 occupied the *trans* state in both leaflets for more than 80% of the simulation, while θ_4 spent most of the simulation in the g^+ state in both leaflets. The analysis again shows differences between the two leaflets, namely the behavior of the θ_1 and θ_2 dihedral angles.

Investigation of all possible combinations of θ_2/θ_4 conformers is also of interest because this pair of angles largely determines the orientation of the headgroup with respect to the membrane surface (Pascher et al., 1992). The results show that the θ_2/θ_4 pair spent 50.8% of the simulation in the *trans*/*gauche*$^+$ state. For the rest of the simulation θ_2/θ_4 occupied the *gauche*$^\pm$/*gauche*$^\pm$ state (14.5% of the simulation in the g^+/g^+ state, 20.3% in the g^-/g^+ state, and 14.4% in the g^-/g^- state). Experiments on the crystalline phase of DMPC indicate that the *gauche*$^\pm$/*gauche*$^\pm$ combination of these two angles is dominant in the crystal state (Pascher et al., 1992) in contrast to the fluid phase simulation results, which indicate almost equal populations of both the *trans*/*gauche*$^+$ and *gauche*$^\pm$/*gauche*$^\pm$ states for the θ_2/θ_4 pair.

The conformation of the headgroup choline moiety was characterized in terms of the five dihedral angles α_i (i = 1, 2, 3, 4, 5). The angles α_4 and α_5 influence not only the overall headgroup conformation and its orientation, but also the distance between the atoms P and N. Torsions around the remaining α_i (i = 1, 2, 3) dihedral angles are not restricted by significant energetic barriers (Woolf and Roux, 1994b). The isomerization rates of the α_1 to α_5 angles range from 1.1 ns^{-1} (for α_5) to 31.0 ns^{-1} (for α_3) in the upper leaflet, and from 3.1 ns^{-1} (for α_1) to 21.9 ns^{-1} (for α_3) in the lower leaflet (see Table 5). Thus the most mobile angle in both leaflets appears to be α_3, with isomerization rates comparable to those of dihedral angles of the hydrocarbon chains. The most rigid angle in the upper leaflet is α_5, with isomerization rates comparable to those of the dihedral angles of the glycerol region, while in the lower leaflet it is α_1. The fractions of the α_i dihedral angles occupying individual states were compared to those determined by Egberts et al. (1994), who performed an MD simulation of a neat DPPC bilayer at 350 K. The agreement was very good for α_1 and α_3, but significant differences were observed for α_2, α_4, and α_5. The relative occupancies of the *gauche* states by the α_2 and α_4 dihedral angles were approximately 1.8 and 1.3 times larger in this study. The relative occupancy of the *trans* state by α_5 was ~50% larger here (80.5%, averaged over both leaflets) compared to the observation of Egberts et al. (1994) that α_5 spent 57% of the simulation in one or the other of the two *gauche* states. Experimental studies, x-ray crystallography (Sundaralingam, 1972; Hauser et al., 1981), ^{2}H-NMR (Seelig, 1978), Raman, and ^{1}H-NMR (Akutsu, 1981) indicate that α_5 is predominantly in the *gauche* state.

TABLE 4 Average occupancy of the glycerol backbone dihedral angles

	Upper Leaflet			Lower Leaflet		
Dihedral Angle	% g^+	% g^-	% *trans*	% g^+	% g^-	% *trans*
α_1	13.5	0	86.5	8.8	26	65.2
α_2	0.1	51.2	48.7	38.6	17.1	44.3
α_3	9.6	47.1	43.1	50.5	33.7	15.7
α_4	0.04	0.4	99.5	8	10.4	81.6
α_5	0.1	0.1	99.7	28.3	10.4	61.3
θ_1	59.5	14.9	25.6	42.2	14	43.8
θ_2	14.9	25.6	59.5	14	43.8	42.2
θ_3	12.1	0	87.9	16.7	0	83.3
θ_4	87.9	12	0	83.3	16.7	0

The definition of the different angles is given in the text and in Fig. 10.

TABLE 5 Isomerization rates of the dihedral angles α_i defining the conformation of the choline part of the lipid headgroups

Dihedral Angle	Upper Leaflet	Lower Leaflet
α_1	3.3	3.1
α_2	2.5	5.5
α_3	31.0	21.9
α_4	1.3	8.0
α_5	1.1	9.7

The definition of the different angles is given in the text and in Fig. 10.

The discrepancies in the headgroup structures in the two simulation studies may be due to the different compositions of the two systems, i.e., the presence of the peptide may have caused observed structural changes of the headgroups compared to a simple DPPC bilayer. This conclusion is supported by ^{2}H-NMR experiments performed on a system composed of a similar synthetic amphiphilic peptide (peptide-20) incorporated into DMPC bilayers at a peptide/lipid molar ratio of 1:30 at a temperature of 34°C using DMPC, which was selectively deuterated at the headgroup α and β positions (the notation of α and β positions in a lipid headgroup is: $-O_3-POCH_2^{(\alpha)}CH_2^{([\beta])}N(CH_3)_3^+$) (Roux et al., 1989). They found large changes of the quadrupolar splittings of the choline headgroups and concluded that in the presence of the amphiphilic peptide-20 the DMPC headgroups underwent a conformational change, leading to a change in its average orientation. Similar measurements on mixtures of pentalysine with DMPC showed no such behavior (Roux et al., 1989). These results were interpreted in terms of an electrostatic torque acting on the lipid headgroup dipole moment due to surface charge embedded at different levels within the membrane. The trans-membrane peptide, having its charges more deeply buried within the lipid bilayer, caused a significant change in headgroup orientation, while the pentalysine peptide, which rests higher on the membrane surface, had little effect. This may also explain the asymmetry observed in the present simulation since the charged lysines at the N-terminus (the lower leaflet) extend further into the water (and covers a wider range in z) than those near the C-terminus (the upper leaflet) (compare Figs. 1 and 11).

Solvation of the lipid headgroups

The analysis of the average orientation of the PN dipoles with respect to the bilayer normal implied that the PN dipoles point into the water phase on average, suggesting that the headgroups were probably solvated by water molecules. In order to test this assertion, radial distribution functions of water oxygens about nitrogen, phosphorus, and phosphoryl oxygens were calculated and are shown in Fig. 12. The radial distribution functions about nitrogen and phosphorus indicate that these atoms do not interact strongly with the water, as the first maximum is located at ~4 Å for both P and N. A similar distribution of water oxygens about the nitrogen of the trimethylammonium group of the DMPC headgroup in a hydrated DMPC bilayer at 327 K was reported by Damodaran and Merz (1993). However, the radial distribution functions for both O_{13} and O_{14} are sharply peaked at ~2.7 Å, indicating the formation of a well-defined first hydration shell.

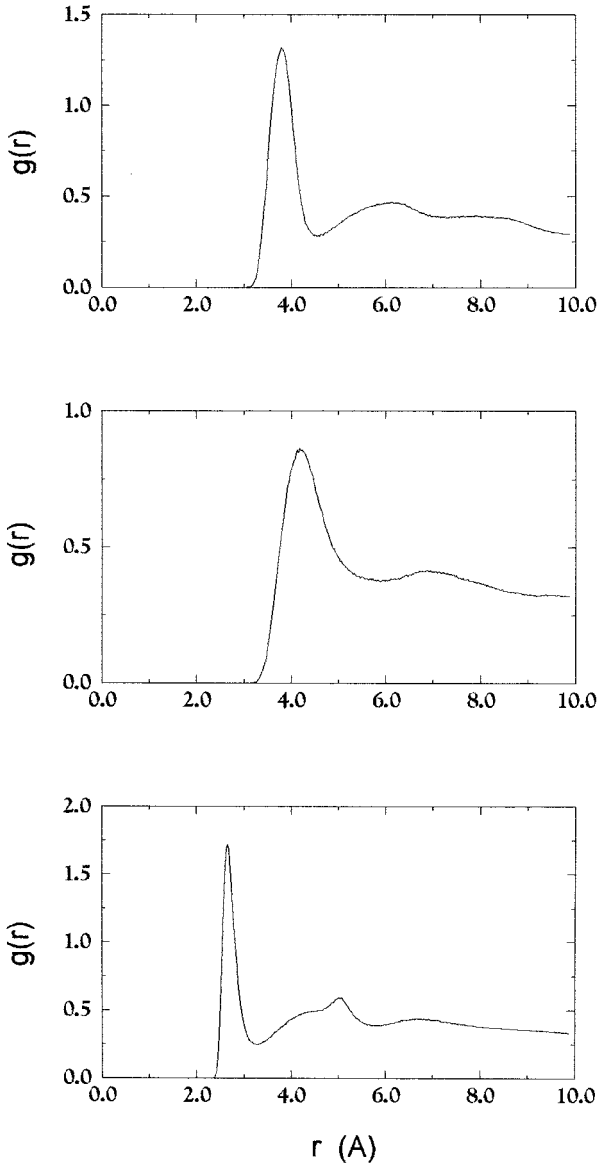

FIGURE 12 The radial distribution functions of water oxygens about (*top*) the phosphorus, (*middle*) the nitrogen, and (*bottom*) the phosphoryl oxygens (O13, O14) in the lipid headgroups, averaged over all lipids.

The association of the peptide amide hydrogens with the lipid phosphoryl oxygens was also investigated in order to find out if there was any possibility of long-term hydrogen bonding between these atoms. The radial distribution functions of O_{13} of DMPC 11 about the peptide's first three

amide protons, HN_1, HN_2, and HN_3, indicated the possible occurrence of hydrogen bonds between O_{13} and these amide hydrogens. A more detailed analysis revealed that during the first 400 ps all three amide protons were hydrogen-bonded to this oxygen atom for at least part of the time, HN_1 for 33.7% of the simulation, HN_2 for 18.2% of the simulation, and HN_3 for 21.5% of the simulation (a hydrogen bond was assumed to exist if the distance between the hydrogen and oxygen was <2.5 Å and if the nitrogen-hydrogen-oxygen angle was $>135°$; Kovacs et al., 1995).

CONCLUSION

By using molecular dynamics simulation of the simple trans-bilayer peptide-16 in fully hydrated DMPC and ^{2}H-NMR spectroscopy of mixtures of the same peptide-16 with DMPC and of the related peptide-24 with DMPC and DPPC, we have shown that there is a substantial ordering of the lipid chains due to the peptide when the helical length of the peptide is greater than the normal lipid bilayer thickness. We have identified a number of differences in the lipid dynamics observed with this simulation and previous simulations on lipid bilayer systems that may also be due to the influence of the peptide. Further studies of model membrane systems both with and without trans-bilayer peptides, and as a function of peptide length and concentration, performed under identical conditions, would help to clarify the importance of lipid-peptide interactions on membrane molecular properties.

Through comparison of average quantities calculated from the simulation coordinate files with experimental observation, a number of research groups have shown that MD simulations provide a good description of model membrane molecular order and dynamics. Full-atom molecular dynamics simulations of complex multicomponent systems such as membranes can provide a precise and reliable description of these systems provided they have been carefully constructed and equilibrated. Although it is true that construction of the simulation system in a manner which immediately is consistent with known properties, such as the lipid chain order profile, may bias the results of these short time scale simulations (1 ns), the agreement between similar systems simulated by different groups, using different assembly techniques and different boundary conditions, implies that generally such simulations faithfully represent the experimental systems. The agreement among simulations of similar systems and between simulation and experiment is gratifying, and the impressive improvements in system size and simulation time scale being made possible by each succeeding generation of computers is making more detailed and precise comparisons possible. One obvious but important extension to the current scale of these simulations is to increase the length of the simulation by at least an order of magnitude to allow the sampling of slower processes and to provide better statistics on those processes already being sampled. Another is to significantly increase the size of the unit cell, i.e., the number of molecules being simulated. This will also provide better statistics for all the properties being calculated. Finally, with continual improvements in computer speed and accessibility (i.e., lower cost) it should be possible to address these two issues and to begin to perform computer "experiments" wherein important variables such as temperature, pressure, and even composition are systematically varied so that their effect on system properties can be evaluated and compared to experimental measurements.

We thank Professors Bernie Nickel, of the Physics Department at the University of Guelph, Benoit Roux, of the Departments of Chemistry and Physics at the Université de Montréal, and Thomas Woolf, of the Department of Physiology at Johns Hopkins University. We also thank Christophe Fares for help in making the figures.

This work was supported by grants from the Natural Sciences and Engineering Research Council of Canada.

REFERENCES

Ahlstrom, P., and H. J. C. Berendsen. 1993. A molecular dynamics study of lecithin monolayers. *J. Phys. Chem.* 97:13691–13702.

Akutsu, H. 1981. Direct determination by Raman scattering of the conformation of the choline group in phospholipid bilayers. *Biochemistry.* 20:7359–7366.

Belohorcova, K., and J. H. Davis. 1998. Molecular dynamics simulations of model membranes. *In* Biomembrane Structures, D. Chapman and P. I. Haris, editors. IOS Press, Amsterdam, The Netherlands.

Belohorcova, K., J. H. Davis, T. B. Woolf, and B. Roux. 1997. Structure and dynamics of an amphiphilic peptide in a lipid bilayer: A molecular dynamics study. *Biophys. J.* 73:3039–3055.

Berneche, S., M. Nina, and B. Roux. 1998. Molecular dynamics simulation of melittin in a dimyristoylphosphatidylcholine bilayer membrane. *Biophys. J.* 75:1603–1618.

Bloom, M., J. H. Davis, and A. L. MacKay. 1981. Direct determination of the oriented sample NMR spectrum from the powder pattern spectrum for systems with local axial symmetry. *Chem. Phys. Lett.* 80:192–202.

Brooks, B. R., R. E. Bruccoleri, B. D. Olafson, D. J. States, S. Swaminathan, and M. Karplus. 1983. CHARMM: a program for macromolecular energy, minimization and dynamics calculations. *J. Comput. Chem.* 4:187–217.

Brown, M. F. 1994. Modulation of rhodopsin function by properties of the membrane bilayer. *Chem. Phys. Lipids.* 104:5497–5509.

Büldt, G., and R. Wohlgemuth. 1981. The headgroup conformation of phospholipids in membranes. *J. Membr. Biol.* 58:81–100.

Cevc, G., and D. Marsh. 1987. Phospholipid Bilayers: Physical Principles and Models. John Wiley and Sons, New York.

Chiu, S.-W., M. Clark, V. Balaji, S. Subramaniam, H. L. Scott, and E. Jacobsson. 1995. Incorporation of surface tension into molecular dynamics simulation of an interface: a fluid phase lipid bilayer membrane. *Biophys. J.* 69:1230–1245.

Chiu, S.-W., L. K. Nicholson, M. T. Brenneman, S. Subramaniam, Q. Teng, J. A. McCammon, T. A. Cross, and E. Jacobsson. 1991. Molecular dynamics computations and solid state nuclear magnetic resonance of the gramicidin cation channel. *Biophys. J.* 60:974–978.

Cross, T. A. 1994. Structural biology of peptides and proteins in synthetic membrane environments by solid-state NMR spectroscopy. *Annu. Rep. NMR Spect.* 29:123–167.

Damodaran, K. V., and K. M. Merz, Jr. 1993. Headgroup-water interactions in lipid bilayers: a comparison between DMPC- and DLPE-based lipid bilayers. *Langmuir.* 9:1179–1183.

Damodaran, K. V., K. M. Merz, and B. P. Gaber. 1995. Interaction of small peptides with lipid bilayers. *Biophys. J.* 69:1299–1308.

Davis, J. H. 1979. Deuterium magnetic resonance study of the gel and liquid crystalline phases of dipalmitoyl phosphatidylcholine. *Biophys. J.* 27:339–358.

Davis, J. H. 1983. The description of membrane lipid conformation, order and dynamics by ^{2}H-NMR. *Biochem. Biophys. Acta.* 737:117–171.

Davis, J. H. 1991. Deuterium nuclear magnetic resonance spectroscopy in partially ordered systems. *In* Isotopes in the Physical and Biomedical Sciences, vol. 2, E. Buncel and J. R. Jones, editors. Elsevier Science Publishers B. V., Amsterdam. 99–157.

Davis, J. H., and M. Auger. 1999. Static and magic angle spinning NMR of membrane peptides and proteins. *J. Prog. NMR Spect.* 35:1–84.

Davis, J. H., D. M. Clare, R. S. Hodges, and M. Bloom. 1983. Interaction of a synthetic amphiphilic polypeptide and lipids in a bilayer structure. *Biochemistry.* 22:5298–5305.

Davis, J. H., K. R. Jeffrey, M. Bloom, M. I. Valic, and T. P. Higgs. 1976. Quadrupolar echo deuterium nuclear magnetic resonance spectroscopy in ordered hydrocarbon chains. *Chem. Phys. Lett.* 42:390–394.

De Loof, H., S. C. Harvey, J. P. Segrest, and R. W. Pastor. 1991. Mean field stochastic boundary molecular dynamics simulation of a phospholipid in a membrane. *Biochemistry.* 30:2099–2113.

de Planque, M. R. R., D. V. Greathouse, R. E. Koeppe II, H. Schafer, D. Marsh, and J. A. Killian. 1998. Influence of lipid/peptide hydrophobic mismatch on the thickness of diacylphosphatidylcholine bilayers. A ^{2}H-NMR and ESR study using designed transmembrane α-helical peptides and gramicidin A. *Biochemistry.* 37:9333–9345.

Douliez, J.-P., A. Leonard, and E. J. Dufourc. 1995. Restatement of order parameters in biomembranes: calculation of C-C bond order parameters from C-D quadrupolar splittings. *Biophys. J.* 68:1727–1739.

Dumas, F., J.-F. Tocanne, G. Leblanc, and M.-C. Lebrun. 2000. Consequences of hydrophobic mismatch between lipids and melibiose permease on melibiose transport. *Biochemistry.* 39:4846–4854.

Duneau, J.-P., S. Crouzy, N. Garnier, Y. Chapron, and M. Genest. 1999. Molecular dynamics simulations of the Erb-B2 transmembrane domain within an explicit membrane environment: comparison with vacuum simulations. *Biophys. Chem.* 76:35–53.

Edholm, O., O. Berger, and F. Jahnig. 1995. Structure and fluctuations of bacteriorhodopsin in the purple membrane: a molecular dynamics study. *J. Mol. Biol.* 250:94–111.

Egberts, E., S. J. Marrink, and H. J. C. Berendsen. 1994. Molecular dynamics simulation of a phospholipid membrane. *Eur. Biophys. J.* 22:423–436.

Essman, U., and M. L. Berkowitz. 1999. Dynamical properties of phospholipid bilayers from computer simulation. *Biophys. J.* 76:2081–2089.

Feller, S. E., Y. Zhang, R. W. Pastor, and B. R. Brooks. 1995. Constant pressure molecular dynamics simulation: the Langevin piston method. *J. Chem. Phys.* 103:4613–4621.

Finnean, J. B., R. Coleman, and R. H. Michell. 1978. Membranes and their Cellular Functions. 2nd Ed. Blackwell, Oxford.

Franks, N. P. 1976. Structural analysis of hydrated egg lecithin and cholesterol bilayers. *J. Mol. Biol.* 100:345–358.

Haile, J. M. 1992. Molecular Dynamics Simulations: Elementary Methods. John Wiley and Sons, New York.

Harroun, T. A., W. T. Heller, T. M. Weiss, L. Yang, and H. W. Huang. 1999a. Experimental evidence for hydrophobic matching and membrane-mediated interactions in lipid bilayers containing gramicidin. *Biophys. J.* 76:937–945.

Harroun, T. A., W. T. Heller, T. M. Weiss, L. Yang, and H. W. Huang. 1999b. Theoretical analysis of hydrophobic matching and membrane-mediated interactions in lipid bilayers containing gramicidin. *Biophys. J.* 76:3176–3185.

Hauser, H., I. Pascher, R. H. Pearson, and S. Sundell. 1981. Preferred conformation and molecular packing of phosphatidylethanolamine and phosphatidylcholine. *Biochim. Biophys. Acta.* 650:21–51.

Helfand, E. 1978. Brownian dynamics study of transitions in a polymer chain of bistable oscillators. *J. Chem. Phys.* 69:1010–1018.

Hinz, H.-J., and J. M. Sturtevant. 1972. Calorimetric studies of dilute aqueous suspensions of bilayers formed from synthetic L-α-lecithins. *J. Biol. Chem.* 247:6071–6075.

Hitchcock, P. B., R. Mason, and G. G. Shipley. 1975. Phospholipid arrangements in multilayers and artificial membranes: quantitative analysis of the x-ray diffraction data from a multilayer of 1,2-dimyristoyl-DL-phosphatidylethanolamine. *J. Mol. Biol.* 94:297–299.

Hoult, D. I., and R. E. Richards. 1975. Critical factors in design of sensitive high-resolution nuclear magnetic resonance spectrometers. *Proc. R. Soc. Lond. A.* 344:311–340.

Huang, P., and G. H. Loew. 1995. Interaction of an amphiphilic peptide with a phospholipid bilayer surface by molecular dynamics simulation study. *J. Biomol. Struct. Dyn.* 12:937–956.

Huschilt, J. C., R. S. Hodges, and J. H. Davis. 1985. Phase equilibria in an amphiphilic peptide-phospholipid model membrane by deuterium nuclear magnetic resonance difference spectroscopy. *Biochemistry.* 24: 1377–1386.

Huschilt, J. C., B. Millman, and J. H. Davis. 1989. Orientation of α-helical peptides in a lipid bilayer. *Biochim. Biophys. Acta.* 979:139–141.

Kerr, I. D., R. Sankararamakrishnan, J. D. Madura, R. W. Impey, and M. L. Klein. 1994. Parallel helix bundles and ion channels. Molecular modeling via simulated annealing and restrained molecular dynamics. *Biophys. J.* 67:1501–1515.

Ketchem, R. R., K.-C. Lee, S. Huo, and T. A. Cross. 1996. Macromolecular structural elucidation with solid-state NMR derived orientational constraints. *J. Biomolec. NMR.* 8:1–14.

Kimmich, R., G. Schnur, and A. Scheuermann. 1983. Spin-lattice relaxation and lineshape parameters in nuclear magnetic resonance of lamellar lipid systems: fluctuation spectroscopy of disordering mechanisms. *Chem. Phys. Lipids.* 2:271–322.

Kovacs, H., A. E. Mark, J. Johansson, and W. F. van Gunsteren. 1995. The effect of environment on the stability of an integral membrane helix: molecular dynamics simulations of surfactant protein C in chloroform, methanol and water. *J. Mol. Biol.* 247:808–822.

Leach, A. R. 1997. Molecular Modelling: Principles and Applications. Chap. 6. Addison-Wesley Longman, Ltd., Harlow, UK.

Lewis, B. A., and D. M. Engelman. 1983. Lipid bilayer thickness varies linearly with acyl chain length in fluid phosphatidylcholine vesicles. *J. Mol. Biol.* 166:211–217.

Mackerell, A. D., D. Bashford, M. Bellot, R. L. Dunbrack, M. J. Field, S. Fischer, J. Gao, H. Guo, D. Joseph, S. Ha, L. Kuchnir, K. Kuczera, F. T. K. Lau, C. Mattos, S. Michnick, D. T. Nguyen, T. Ngo, B. Prodhom, B. Roux, B. Schlenkrich, J. Smith, R. Stote, J. Straub, J. Wiorkiewicz-Kuczera, and M. Karplus. 1992. Self-consistent parametrization of biomolecules for molecular modeling and condensed phase simulations. *Biophys. J.* 61:143*a*. (Abstr.).

Marrink, S.-J., M. Berkowitz, and H. J. C. Berendsen. 1993. Molecular dynamics simulation of a membrane/water interface: the ordering of water and its relation to the hydration force. *Langmuir.* 9:3122–3131.

Meier, P., E. Ohmes, and G. Kothe. 1986. Multipulse dynamic nuclear magnetic resonance of phospholipid membranes. *J. Chem. Phys.* 85: 3598–3614.

Mendelsohn, R., M. A. Davies, J. W. Brauner, H. F. Schuster, and R. A. Dluhy. 1989. Quantitative determination of conformational disorder in the acyl chains of phospholipid bilayers by infrared spectroscopy. *Biochemistry.* 28:8934–8939.

Mendelsohn, R., and R. G. Snyder. 1996. Infrared spectroscopic determination of conformational disorder and microphase separation in phospholipid acyl chains. *In* Biological Membranes. K. Merz and B. Roux, editors. Birkhauser, Boston. 145–174.

Morein, S., R. E. Koeppe II, G. Lindblom, B. de Kruijff, and J. Antoinette Killian. 2000. The effect of peptide/lipid hydrophobic mismatch on the phase behavior of model membranes mimicking the lipid composition in *Escherichia coli* membranes. *Biophys. J.* 78:2475–2485.

Morrow, M. R., and J. H. Davis. 1988. Differential scanning calorimetry and ^{2}H-NMR studies of the phase behaviour of gramicidin-phosphatidylcholine mixtures. *Biochemistry.* 27:2024–2032.

Morrow, M. R., J. C. Huschilt, and J. H. Davis. 1985. Simultaneous modeling of phase and calorimetric behaviour in an amphiphilic peptide/phospholipid model membrane. *Biochemistry.* 24:5396–5406.

Mouritsen, O. G., and M. Bloom. 1984. Mattress model of lipid-protein interactions in membranes. *Biophys. J.* 46:141–153.

Nagle, J. F. 1993. Area/lipid of bilayers from NMR. *Biophys. J.* 64: 1476–1481.

Nagle, J. F., R. Zhang, S. Tristram-Nagle, W. Sun, H. I. Petrache, and R. M. Suter. 1996. X-ray structure determination of fully hydrated L alpha phase dipalmitoylphosphatidylcholine bilayers. *Biophys. J.* 70: 1419–1431.

Nelander, J. C., and A. E. Blaurock. 1978. Disorder in nerve myelin: phasing the higher order reflections by means of the diffuse scatter. *J. Mol. Biol.* 118:497–532.

North, C. L., and T. A. Cross. 1995. Correlations between function and dynamics: time scale coincidence for ion translocation and molecular dynamics in the gramicidin channel backbone. *Biochemistry.* 34: 5883–5895.

Oldfield, E., M. Meadows, D. Rice, and R. Jacobs. 1978. Spectroscopic studies of specifically deuterium labeled membrane systems. Nuclear magnetic resonance investigation of the effects of cholesterol in model systems. *Biochemistry.* 17:2727–2740.

Pascher, I., M. Lundmark, P.-G. Nyholm, and S. Sundell. 1992. Crystal structures of membrane lipids. *Biochim. Biophys. Acta.* 1113:339–373.

Pasenkiewicz-Gierula, M., Y. Takaoka, H. Mihagawa, K. Kitamura, and A. Kusumi. 1999. Charge pairing of headgroups in phosphatidylcholine membranes: a molecular dynamics simulation study. *Biophys. J.* 76: 1228–1240.

Pastor, R. W., and S. E. Feller. 1996. Time scales of lipid dynamics and molecular dynamics. *In* Biological Membranes: A Molecular Perspective from Computation and Experiment. K. M. Merz, Jr., and B. Roux, editors. Birkhauser, Boston. 3–29.

Pastor, R. W., R. H. Venable, and M. Karplus. 1991. Model for the structure of the lipid bilayers. *Proc. Natl. Acad. Sci. U.S.A.* 88:892–896.

Pauls, K. P., A. L. MacKay, O. Söderman, M. Bloom, A. K. Tanjea, and R. S. Hodges. 1985. Dynamics properties of the backbone of an integral membrane polypeptide measured by ^{2}H-NMR. *Eur. Biophys. J.* 12:1–11.

Pink, D., T. J. Green, and D. Chapman. 1980. Raman scattering in bilayers of saturated phosphatidylcholines. Experiment and theory. *Biochemistry.* 19:349–356.

Prosser, R. S., and J. H. Davis. 1994. Dynamics of an integral membrane protein: a deuterium NMR relaxation study of gramicidin. *Biophys. J.* 66:1429–1440.

Prosser, R. S., J. H. Davis, C. Mayer, K. Weisz, and G. Kothe. 1992. Deuterium NMR relaxation studies of peptide-lipid interactions. *Biochemistry.* 31:9355–9363.

Prosser, R. S., S. I. Daleman, and J. H. Davis. 1994. The structure of an integral membrane peptide: a deuterium NMR study of gramicidin. *Biophys. J.* 66:1415–1428.

Rappaport, D. C. 1995. The Art of Molecular Dynamics Simulation, Chap. 6. Cambridge University Press, Cambridge, UK.

Robinson, A. J., W. G. Richards, P. J. Thomas, and M. M. Hann. 1994. Headgroup and chain behavior in biological membranes: a molecular dynamics computer simulation. *Biophys. J.* 67:2345–2354.

Roux, M., J.-M. Neumann, R. S. Hodges, P. F. Devaux, and M. Bloom. 1989. Conformational changes of phospholipid headgroups induced by a cationic integral membrane peptide as seen by deuterium magnetic resonance. *Biochemistry.* 28:2313–2321.

Roux, B., and T. B. Woolf. 1996. Molecular dynamics of Pf1 coat protein in a phospholipid bilayer. *In* Biological Membranes: A Molecular Perspective from Computation and Experiment. K.M. Merz, Jr. and B. Roux, editors. Birkhauser, Boston. 555–587.

Ryckaert, J.-P., G. Ciccotti, and H. J. C. Berendsen. 1977. Numerical integration of the Cartesian equations of motion of a system with constraints: molecular dynamics of n-alkanes. *J. Comput. Phys.* 23: 327–341.

Schindler, H., and J. Seelig. 1975. Deuterium order parameters in relation to thermodynamic properties of a phospholipid bilayer. A statistical mechanical interpretation. *Biochemistry.* 14:2283–2287.

Seelig, J. 1978. Nuclear magnetic resonance and the headgroup structure of phospholipids in membranes. *Biochim. Biophys. Acta.* 515:105–140.

Seelig, J., H.-U. Gaily, and R. Wohlgemuth. 1977. Orientation and flexibility of the choline headgroup in phosphatidylcholine bilayers. *Biochim. Biophys. Acta.* 467:109–119.

Seelig, A., and J. Seelig. 1974. The dynamic structure of fatty acyl chains in a phospholipid bilayer measured by deuterium magnetic resonance. *Biochemistry.* 13:4839–4845.

Seelig, J., and A. Seelig. 1980. Lipid conformation in model membranes and biological membranes. *Q. Rev. Biophys.* 13:19–61.

Shen, L., D. Bassolino, and T. Stouch. 1997. Transmembrane helix structure, dynamics and interactions: multi-nanosecond molecular dynamics simulations. *Biophys. J.* 73:3–20.

Stouch, T. R. 1993. Lipid membrane structure and dynamics studied by all-atom molecular dynamics simulations of hydrated phospholipid bilayers. *Mol. Sim.* 10:335–362.

Sundaralingam, M. 1972. Molecular structures and conformations of the phospholipids and sphingomyelins. *Ann. NY Acad. Sci.* 195:324–355.

Tieleman, D. P., and H. J. C. Berendsen. 1998. A molecular dynamics study of the pores formed by *Escherichia coli* OmpF porin in a fully hydrated palmitoyleoleoylphosphatidylcholine bilayer. *Biophys. J.* 74: 2786–2801.

Tieleman, D. P., H. J. C. Berendsen, and M. S. P. Sansom. 1999a. An alamethicin channel in a lipid bilayer: molecular dynamics simulations. *Biophys. J.* 76:1757–1769.

Tieleman, D. P., H. J. C. Berendsen, and M. S. P. Sansom. 1999b. Surface binding of alamethicin stabilizes its helical structure: molecular dynamics simulations. *Biophys. J.* 76:3186–3191.

Tieleman, D. P., S. J. Marrink, and H. J. C. Berendsen. 1997. A computer perspective of membranes: molecular dynamics studies of lipid bilayer systems. *Biochim. Biophys. Acta.* 1331:235–270.

Tobias, D. J., M. L. Klein, and S. J. Opella. 1993. Molecular dynamics simulation of pf1 coat protein. *Biophys. J.* 64:670–675.

Tobias, D. J., K. Tu, and M. L. Klein. 1997. Atomic-scale molecular dynamics simulations of lipid membranes. *Curr. Opin. Coll. Int. Sci.* 2:15–26.

van der Ploeg, P., and H. J. C. Berendsen. 1983. Molecular dynamics of a bilayer membrane. *Mol. Phys.* 49:233–248.

Venable, R. M., Y. Zhang, B. J. Hardy, and R. W. Pastor. 1993. Molecular dynamics simulations of a lipid bilayer and of hexadecane: an investigation of membrane fluidity. *Science.* 262:223–226.

Verlet, L. 1967. Computer experiments on classical fluids. I. Thermodynamical properties of Lennard-Jones molecules. *Phys. Rev.* 159:98–103.

Wiener, M. C., and S. H. White. 1992a. Structure of a fluid dioleoylphosphatidylcholine bilayer determined by joint refinement of x-ray and neutron diffraction data. II. Distribution and packing of terminal methyl groups. *Biophys. J.* 61:428–433.

Wiener, M. C., and S. H. White. 1992b. Structure of a fluid dioleoylphosphatidylcholine bilayer determined by joint refinement of x-ray and neutron diffraction data. III. Complete structure. *Biophys. J.* 61: 434–447.

Woolf, T. B., and B. Roux. 1994a. Molecular dynamics simulation of the gramicidin channel in a phospholipid bilayer. *Proc. Natl. Acad. Sci. U.S.A.* 91:11631–11635.

Woolf, T. B., and B. Roux. 1994b. Conformational flexibility of *o*-phosphorylcholine and *o*-phosphorylethanolamine: a molecular dynamics study of solvation effects. *J. Am. Chem. Soc.* 116:5916–5926.

Woolf, T. B., and B. Roux. 1996. Structure, energetics and dynamics of lipid-protein interactions: a molecular dynamics study of the gramicidin A channel in a DMPC bilayer. *Proteins.* 24:92–114.

Zhang, Y., and R. W. Pastor. 1994. A comparison of methods for computing transition rates from molecular dynamics simulation. *Mol. Sim.* 13:25–38.